Depth-domain Q compensation

Can Peng, Xuhui Luo, Diancheng Wang, and Jeshurun Hembd, CGG

Summary

Frequency-dependent anelastic attenuation in the earth's crust (the Q effect) is one of the main reasons for bandwidth shrinkage in seismic images and distortion of amplitude versus angle (AVA) response. Therefore, Q compensation is a critical step in seismic processing to achieve good resolution and correct AVA curves for further interpretation. Conventional Q compensation methods (pre-/post-migration) usually over-simplify geological structures or Q models. On the other hand, although Q compensating migration methods are highly accurate in handling complex structures and complex Q models in theory, they can be costly and susceptible to noise and artifact boosting. We propose a post-migration 3D Q compensation process in the depth domain that is accurate for complex geological structures, accommodates complex Q models, and also provides flexibility in noise handling and spectral control that is critical to AVA recovery.

Introduction

A common problem in seismic images is the loss of energy in high frequencies, especially in deep areas, which degrades resolution and distorts AVA response. This can be characterized by a quality factor (Q) model, and Q model-based spectrum balancing is widely used in the industry.

Q compensation is carried out either outside of migration or during migration. Most conventional pre-/post-migration Q compensation methods (van der Baan, 2012; Margrave et al., 2011) explicitly or implicitly assume simple 1D structures and lack the capability to deal with complex structures, due to either the ambiguity of travel paths in pre-migration data or simple depth-to-time stretching in post-migration data. Conversely, Q compensating migration methods can handle complex structures and complex Q models accurately; however, they have relatively high computational costs and face challenges in handling noise (Cavalca et al., 2013, Wu et al., 2017). In practice, we often need a technology that is more accurate than 1D time-domain pre-/post-migration Q compensation methods for complex structures with complex Q models and that is more flexible in noise handling and boosting control than Q compensating migration methods.

We propose a post-migration 3D Q compensation method in the depth domain for common reflection angle and common azimuth seismic images. With the help of ray-tracing-based effective Q and traveltime calculations and 3D space-to-time mapping, the method accommodates both complex Q models and complex geological structures

better than 1D Q compensation. For each common angle seismic volume, a spatially variant effective Q and a traveltime map are calculated, and the compensation is carried out in the depth domain by mapping spatial frequencies to temporal frequencies. Since the process is decoupled from migration, the noise boosting issue can be handled flexibly and effectively.

The next section is devoted to the basic principle and some details of this method. We then present a synthetic data example and a field data example to demonstrate the effectiveness of the method.

Method

Depth-domain Q compensation can be divided into two stages:
- Effective Q and traveltime map calculations using ray-tracing, given the interval Q model, velocity model, and dip fields extracted from the seismic image.
- Q compensation for the seismic image in spatial coordinates with the help of spatial-frequency-to-time-frequency mapping.

The interval Q model, which can be obtained via Q tomography (Xin et al., 2008, Gamar et al., 2015), is required as an input for this process. Similarly to Cavalca et al.'s method (2013), the effective Q and traveltime map for a certain common reflection angle seismic volume can be obtained by ray-tracing for each common image point (CIP). Starting from a CIP with the dip fields picked from the seismic image, A ray pair with given reflection angle and azimuth is shot into the velocity model, and by integrating the interval Q model along the ray paths, the traveltime and effective Q maps can be obtained.

In order to compensate for the Q effect directly in the depth image space, we need to derive the mapping between the spatial frequency domain and the time frequency domain. Figure 1 is an illustration of a reflection at a dipping reflector with a reflection angle of θ. Based on cross-correlation imaging condition, for common reflection angle images, the spatial wavelet along the normal direction is

$$w(\Delta) := w_D(\boldsymbol{x}_0 + \boldsymbol{n}\Delta) = \int s(t_0 - \tau) r\left(\tau + \frac{2\Delta \cos \theta}{c}\right) d\tau, \quad (1)$$

where s is the source wavelet in time, r is the receiver waveform in time, and Δ is the spatial deviation from the central peak of the spatial wavelet along the normal direction. t_0 is the traveltime of the ray reflected at the

Depth-domain Q compensation

center of this event. Taking the Fourier transform of $w(\Delta)$ with respect to Δ, we have

$$W(k_n) = \frac{c}{2\cos\theta} S^*\left(\frac{k_n c}{2\cos\theta}\right) R\left(\frac{k_n c}{2\cos\theta}\right) = \frac{c}{2\cos\theta} S^*(\omega)R(\omega), \quad (2)$$

where $\omega = \frac{k_n c}{2\cos\theta}$, which is the angular frequency, and $k_n = \sqrt{k_x^2 + k_y^2 + k_z^2}$, which is the radial spatial wavenumber. Here we obtain the mapping between the temporal frequency and the radial spatial wavenumber. Therefore, the Q effect can be expressed as the following equation:

$$W'(k_n) = \frac{c}{2\cos\theta} S^*(\omega)R(\omega)e^{i\left(1-\left|\frac{\omega}{\omega_r}\right|^{-\gamma}\right)\omega t_0 - \left|\frac{\omega}{\omega_r}\right|^{-\gamma}\frac{|\omega|t_0}{2Q}}, \quad (3)$$

where Q is the effective Q of the reflection path of the image point under consideration, and t_0 is the traveltime of the reflection path, $\gamma = (\pi Q)^{-1}$ and ω_r is the reference angular frequency. We assume constant effective Q and traveltime for small sub-volumes in the image space, hence for each sub-volume, the Q effect can be compensated for by the local inverse Q filter with the help of 3D spatial FFT and the wavenumber-frequency mapping,

$$d'(\boldsymbol{x}) = FFT^{-1}Q^{-1}\left(\frac{k_n c}{2\cos\theta}, t_0\right) FFT d(\boldsymbol{x}), \quad (4)$$

where d is the input seismic image with Q effect, Q^{-1} is the inverse Q filter in frequency domain, and d' is the seismic image after Q compensation. Although the above derivation is based on the RTM imaging condition, a similar relationship between the radial spatial wavenumber and the temporal frequency is still preserved for Kirchhoff migration images.

To avoid boosting noise, some preprocessing of the input seismic image to separate the signal and noise may be needed. Any de-noising method can be used for this purpose, and only the separated signal part goes through the Q compensation. Here we use a structurally conformal de-noising method.

To keep the method AVA friendly, some editing of the inverse Q filter is needed. Because far offsets (angles) usually suffer stronger Q effects than near and middle offsets (angles), deep sections of far offsets may have very low S/N beyond a certain frequency. No meaningful signal can be recovered for far offsets beyond this frequency, meanwhile near and middle offsets may get proper boosts in this frequency range. If we let all offsets be freely boosted or just set a common boosting limit for all frequencies, the AVA will be skewed from the baseline. Therefore, we put uniform depth-dependent high frequency

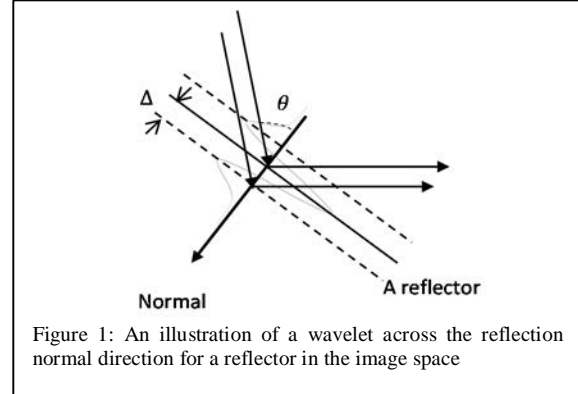limits for all angles, beyond which boosting is not allowed (Trantham and He, 2017).

Figure 1: An illustration of a wavelet across the reflection normal direction for a reflector in the image space

Examples

The first example is based on synthetic data, which is presented to show the validity of this method. The Marmousi model was used in the simulation. The synthetic interval Q model was made by scaling the Marmousi velocity model (Figure 2a and 2b). Wave modeling was carried out on these models, and the seismic image was obtained by performing RTM on the modeled data. We also modeled synthetic data without using the Q model to obtain the image without Q effects with the same processing flow and RTM. This serves as the true answer for Q compensation. The effective Q maps and traveltime maps of different reflection angles were obtained by using ray-tracing on a smoothed Marmousi velocity model and
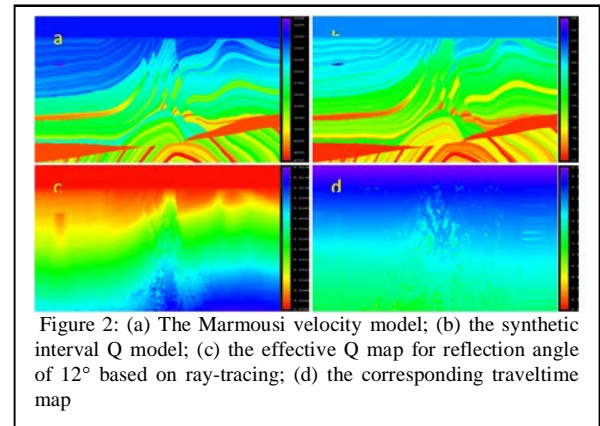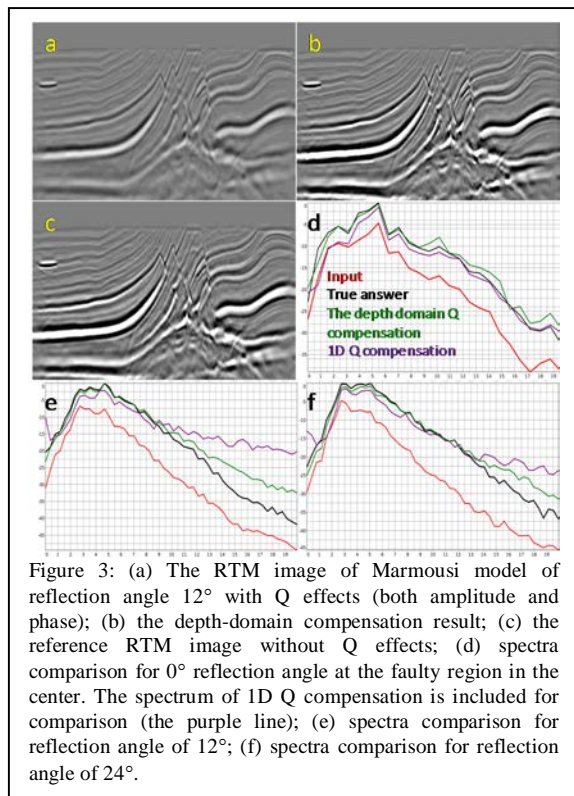

Figure 2: (a) The Marmousi velocity model; (b) the synthetic interval Q model; (c) the effective Q map for reflection angle of 12° based on ray-tracing; (d) the corresponding traveltime map

integrating the interval Q model as discussed in the previous section. The effective Q map and traveltime map of reflection angle of 12° are shown in Figure 2c and Figure 2d.
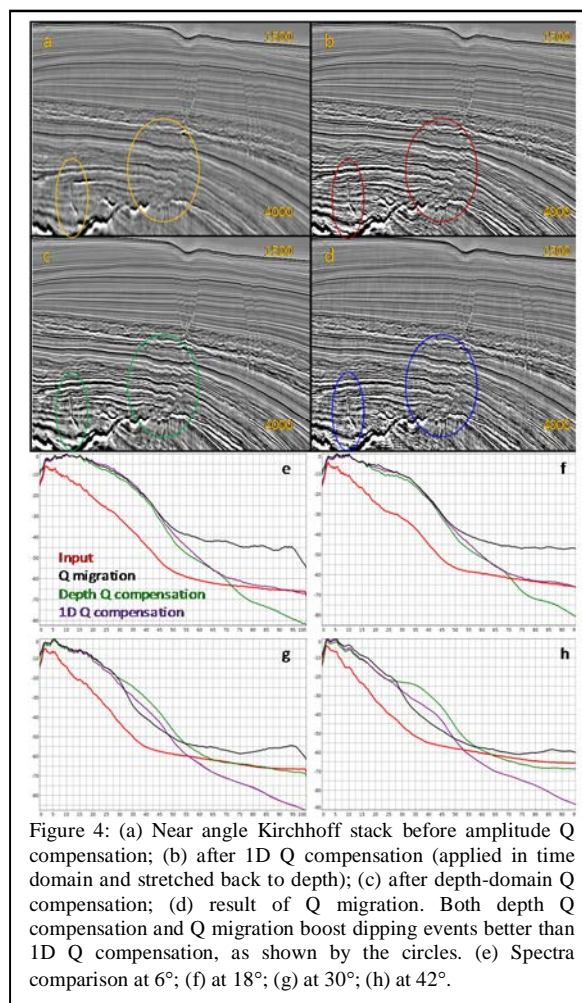
The depth-domain Q compensation result of reflection angle of 12° is shown in Figure 3b. Figure 3a is the

Figure 3: (a) The RTM image of Marmousi model of reflection angle 12° with Q effects (both amplitude and phase); (b) the depth-domain compensation result; (c) the reference RTM image without Q effects; (d) spectra comparison for 0° reflection angle at the faulty region in the center. The spectrum of 1D Q compensation is included for comparison (the purple line); (e) spectra comparison for reflection angle of 12°; (f) spectra comparison for reflection angle of 24°.

seismic image with Q effects and before compensation. The reference image without Q effects is shown in Figure 3c. By comparing Figure 3b against Figure 3c, we can see both amplitude and phase are effectively compensated by the proposed method. Spectra comparisons are shown in Figures 3d, 3e, and 3f for different reflection angles. The spectra are measured at a region with dipping events. In order to show the benefit of 3D depth-domain Q compensation, the spectrum of the 1D Q compensation result is included in the figures. The spectrum of the 3D depth Q compensation result is closer to the reference spectrum than the 1D result, especially at low and middle frequencies. It should be pointed out that the spectra in Figures 3d-f were measured in a 1D fashion; therefore, the energy of the dipping events and faults mainly goes to the low and middle frequencies. The spectrum measurements for different angles also show that this method recovers the AVA characteristics in the main band.

The second example is based on field data from the Santos Basin of offshore of Brazil, where many faults and fine structures are present. The input narrow azimuth data was acquired with variable-depth streamers and went through BroadSeis™ processing. Prestack depth Kirchhoff migration was used to image the data. In order to apply depth-domain Q compensation, surface offset gathers were

Figure 4: (a) Near angle Kirchhoff stack before amplitude Q compensation; (b) after 1D Q compensation (applied in time domain and stretched back to depth); (c) after depth-domain Q compensation; (d) result of Q migration. Both depth Q compensation and Q migration boost dipping events better than 1D Q compensation, as shown by the circles. (e) Spectra comparison at 6°; (f) at 18°; (g) at 30°; (h) at 42°.

converted to reflection angle gathers. To check the advantages of the proposed depth-domain Q compensation, we compare depth-domain Q compensation against 1D post-migration Q compensation and Q Kirchhoff migration using a near angle stack (Figure 4) and depth slices (Figure 5). Dipping events, like faults and fractures, usually challenge 1D methods. When 1D depth-to-time stretch is applied to these events, they appear to be lower frequency than they actually are. Therefore they are usually not compensated sufficiently with 1D methods. As shown in Figures 4b and 5b, due to insufficient boosting, faults and fractures become less salient after Q compensation with the 1D post-migration method. On the other hand, the proposed 3D depth-domain Q compensation and the Q migration can boost faults and fractures correctly. However, for the Q migration, boosting of noise and uncanceled swings is hard to avoid, and it usually destroys some fine structures (Figure 5d). The comparison shows those fine dipping structures are preserved well and can be easily identified
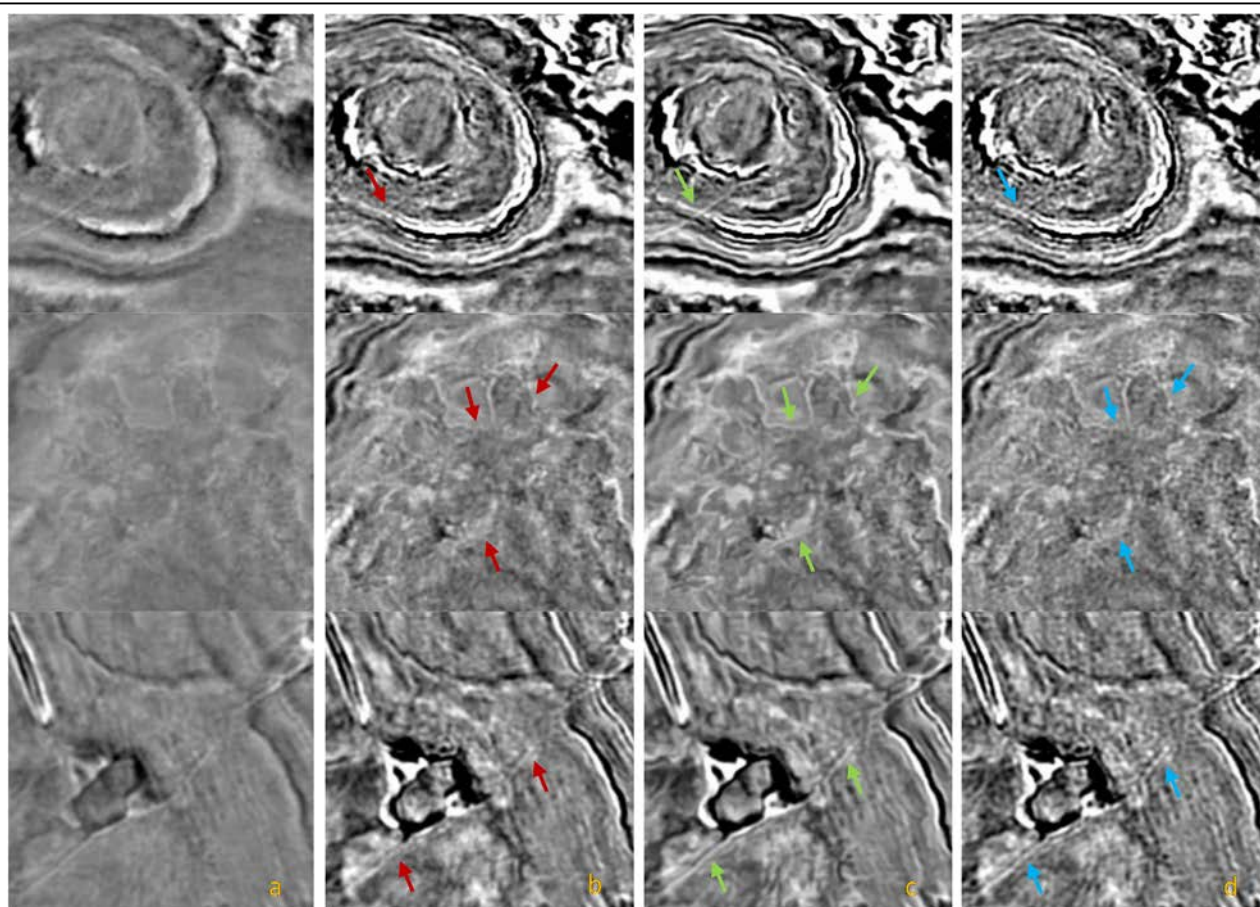
Depth-domain Q compensation

Figure 5: Some depth slices at 3.46 km; column (a) contains 3 depth slices of the near angle Kirchhoff stack before Q compensation; column (b) shows the depth slices after the 1D Q compensation; column (c) shows the depth slices after the depth Q compensation; column (d) shows the results of Q migration. Fine structures in the depth slices are usually caused by dipping events. For 1D methods, they appear to be within a narrow band of low frequencies and get boosted less; therefore, they become less prominent than they should be, as shown in (b). Q migration can sufficiently boost dipping events; however, boosted swings and noise usually destruct these structures, as shown in (d).

after the depth Q compensation, but they become obscure or destructed after 1D Q compensation or Q migration. Figures 4e-4h compare the spectra of the input and outputs of depth-domain Q compensation, 1D Q compensation, and Q migration at four different reflection angles measured within a window at a depth from 3.5 km to 4.5 km.

Conclusions

A post-migration 3D depth-domain Q compensation method is proposed. Compared to previous pre-/post-migration Q compensation methods that are explicitly or implicitly based on the 1D structure assumption, the proposed method accommodates more complex geological structures and Q models with the help of ray-tracing-based effective Q and traveltime estimation. It improves the compensation accuracy at regions with complex geological structures or complex absorption models. On the other

hand, unlike the theoretically precise Q compensating migration methods that incorporate absorption compensation in the imaging process, the proposed method decouples the compensation from the imaging process, and therefore noise suppression and boosting control across different reflection angles can be easily incorporated by post-migration signal and noise separation. This method assumes the traveltime and the effective Q are almost constant within a small spatial volume. Breakdown of this assumption may degrade the accuracy of this method. In the end we need to improve least squares Q migration methods for more precise compensation.

Acknowledgments

REFERENCES

Cavalca, M., R. Fletcher, and M. Riedel, 2013, Q-compensation in complex media– Ray-based and wavefield extrapolation approaches: 83rd Annual International Meeting, SEG, Expanded Abstracts, 3831–3835, https://doi.org/10.1190/segam2013-1130.1.

Gamar, F., D. Carotti, P. Guillaume, A. Cacha, and L. Lopes, 2015, Success of high-resolution volumetric Q tomography in the automatic detection of gas anomalies on offshore Brunei data: 85th Annual International Meeting, SEG, Expanded Abstracts, 5184–5188, https://doi.org/10.1190/segam2015-5865727.1.

Margrave, G. F., M. P. Lamoureux, and D. C. Henley, 2011, Gabor deconvolution: Estimating reflectivity by nonstationary deconvolution of seismic data: Geophysics, **76**, no. 3, W15–W30, https://doi.org/10.1190/1.3560167.

Trantham, E. C., and K. He, 2017, AVA friendly Q amplitude compensation: 87th Annual International Meeting, SEG, Expanded Abstracts, 643–645, https://doi.org/10.1190/segam2017-17073710.1.

van der Baan, M., 2012, Bandwidth enhancement: Inverse Q filtering or time-varying Wiener deconvolution?: Geophysics, **77**, no. 4, V133–V142, https://doi.org/10.1190/geo2011-0500.1.

Wu, X. D., Y. Wang, Y. Xie, J. Zhou, D. Lin, and C. Lorenzo, 2017, Least square Q-Kirchhoff migration: Implementation and application: 79th Annual International Conference and Exhibition, EAGE, Extended Abstracts, Tu A1 08, https://doi.org/10.3997/2214-4609.201700804.

Xin, K., B. Hung, S. Birdus, and J. Sun, 2008, 3-D tomographic amplitude inversion for compensating amplitude attenuation in the overburden: 78th Annual International Meeting, SEG, Expanded Abstracts, 3726–3730, https://doi.org/10.1190/1.3064018.